Standard space co-registration of 3D non-whole brain MRSI and regional metabolic quantification

Xiaodan YAN[1], Ivan Kirov[1], and Oded Gonen[1]
[1]*Radiology, New York University, New York, NY, United States*

Introduction: Magnetic resonance spectroscopy (MRS) and spectroscopic imaging (MRSI) in the human brain are susceptible to: *(i)* repositioning error of the voxel (or grid) in cross-sectional and longitudinal studies; *(ii)* inappropriate choice of region(s) of interest (ROI); and *(iii)* operator error in manual ROI outlining. These problems affect the sensitivity and reliability of MRS and MRSI. To address these issues we *(i)* co-register the 3D MRSI data into standard Talairach space; *(ii)* perform voxelwise statistical analysis on co-registered data from 10 healthy volunteers acquired annually over 3 years (40 data sets); and *(iii)* apply standard-space pre-defined deep brain structures (thalamus, putamen, globus pallidus, posterior cingulate cortex, corpus callosum, centrum semiovale and corona radiata) ROIs to preprocessed metabolic maps to extract average metabolic concentrations.

Methods & Results: Ten healthy volunteers (7 F, 3M) 24 to 43 (mean 30) years old participated in the study after giving their Institutional Review Board approved written informed consent. All experiments were conducted on a 3T Siemens scanner with a TEM3000 circularly-polarized, transmit-receive head-coil (MRI Instruments, Minneapolis, MN). For image-guidance, MP-RAGE images were acquired with: TE/TI/TR= 2.6/800/1360 ms, 256×256×160 mm^3 FOV and 256×256×160 matrix. A 10 cm anterior-posterior (AP) ×8 cm left-right (LR) ×4.5 cm inferior-superior (IS) =360 cm^3 VOI was then image-guided to be centered on the corpus callosum and aligned in the same angle as the MRI. The VOI was then excited using PRESS (TE=35 *ms*) with three second-order Hadamard encoded 1.5 cm thick slabs (6 slices) that were sequentially multiplexed along the IS direction every 1800 ms TR. This optimizes both the SNR and spatial coverage [1] and the thinness of these slabs allowed us to apply strong, 6 mT/m, Hadamard slice select gradients that reduced the ~1.6 ppm (=200 Hz) chemical shift displacement between NAA and mI to ~0.6 mm, less than 8% of the 7.5 mm slices' width. The slices' planes were encoded with 16×16 2D-CSI over a 16×16 cm^2 (LR×AP) FOV. The ^{1}H-MRSI data was reconstructed using in-house IDL software (Research Systems Inc. Boulder CO). After voxel-shifting in the LR×AP planes to align the NAA grid with the VOI, the data was Fourier transformed in the time, AP and LR dimensions, and Hadamard reconstructed along the IS direction. The VOI spectra were then each frequency-aligned and zero-order phased in reference to the NAA peak. The relative levels of the *i*-th (*i*=NAA, Cr, Cho, *m*I, Glu) metabolite in the *j*-th (*j*=1…480) voxel and *k*-th (*k*=1...40) measurement were estimated from their peak area, S_{ijk}, using the SITools-FITT parametric spectral modeling package (using aspartate, glutamate (Glu), glutamine, Cho, Cr, *m*I, NAA and taurine functions) of Soher et al.[2]. Each 16×16×6 S_{ijk} matrices were then linearly interpolated and co-registered to MP-RAGE images, using our in-house Matlab software. The anatomical images of each individual were registered to the Talairach space [3] after skull-stripping. The 40 (10 subjects × 4 measurements each) co-registered maps were averaged, giving rise to Fig.1 middle plane, in which the anatomical landmarks were better demonstrated in the average compared to individual maps (left plane). CSF correction was applied in a voxelwise fashion by dividing S_{ijk} by the CSF probability generated by SPM. Spatial distribution of variance was studied with coefficient-of-variation (CV) and 2-Way analysis of variance (ANOVA); overall variance was demonstrated by CV whereas inter-subject variance was extracted with ANOA (Fig.2). Most of the variance is at the volume-of-interest (VOI) edges due to positioning differences; within the VOI, CSF partial volume is the primary source of variance, followed by cross-subject fine scale variance at gyri and sulci (Fig.2).

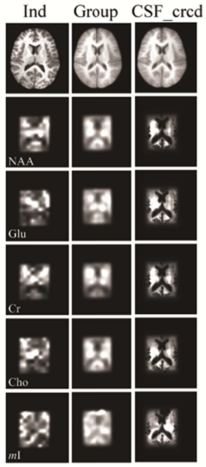

Fig.1: Effect of co-reigstration and CSF correction. Left: individual images; middle: group average after co-registration. Right: Group t maps after CSF correction.

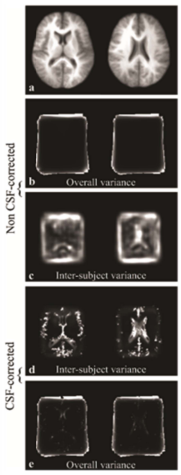

Fig.2: Voxelwise analysis of variance distribution, with CV(b,e)and ANOVA (c,d) demonstrating overal variance and inter-subject variance respectively before (b,c) and after CSF correction (d,e)

ROI		Volume [mm^3]	Metabolic concentration [mM] (mean±SD)				
			NAA	Cr	Cho	*m*I	Glu
Thalamus	L	7531	6.8±1.2	5.2±0.9	1.2±0.2	3.9±0.7	5.5±1.1
	R	7529	6.9±1.1	5.3±0.9	1.2±0.2	3.9±0.8	5.4±1.0
Putamen	L	6231	4.1±1.3	3.4±1.0	0.6±0.2	2.3±0.6	4.0±1.2
	R	6151	4.6±1.0	4.1±0.9	0.8±0.2	2.9±1.2	4.3±1.0
Globus pallidus	L	2265	2.6±1.3	2.1±1.1	0.4±0.2	1.7±0.9	2.6±1.4
	R	2378	2.9±1.3	2.3±1.1	0.5±0.2	1.9±1.0	2.8±1.3
Caudate	L	4439	4.1±1.2	3.7±1.0	0.7±0.2	2.8±0.8	4.1±1.1
	R	4361	4.1±1.4	3.7±1.3	0.8±0.3	3.3±1.7	4.1±1.3
Posterior cingulate	L	6917	6.9±1.3	4.4±0.9	0.8±0.2	3.9±1.0	5.2±0.9
	R	7215	7.4±1.2	4.8±1.0	0.8±0.2	4.2±1.1	5.6±1.0
Centrum semiovale	L	8202	6.8±1.5	4.5±1.0	1.2±0.3	4.1±1.0	4.7±1.1
	R	7648	6.6±1.6	4.3±1.0	1.2±0.3	4.1±1.1	4.2±1.1
Corona radiata	L	4093	7.8±1.5	5.1±1.0	1.3±0.3	4.2±0.8	5.2±1.1
	R	4422	7.7±0.8	5.2±0.6	1.4±0.2	4.4±0.7	4.8±0.7
Corpus callosum		20933	5.2±1.5	3.2±0.9	0.9±0.2	3.6±1.2	4.2±1.0

Table 1: Metabolic concentration in the 15 ROI-s.

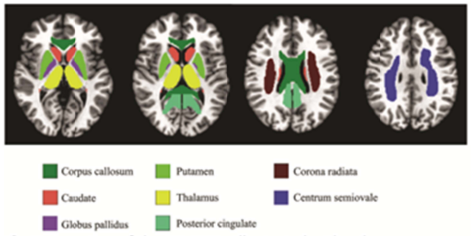

Fig.3: Location of the 3D ROI-s illustrated with color.

Fifteen 3D binary ROI masks whose elements are M_{jm} (*m*=1..15), were obtained in standard space including the left and right parts of five predominantly gray matter structures (putamen, thalamus, caudate, globus pallidus and posterior cingulate cortex); and three white matter structures (corpus callosum, left and right centrum semiovale and corona radiata) (Fig.3)

The concentration in the *m*-th ROI for the *i*-th metabolite in the *k*-th measurement, C_{ikm}, was obtained relative to a 2 L sphere of Ci^{vitro}=12.5, 10.0, 3.0, 7.5 and 12.5 mM NAA, Cr, Cho, mI and Glu in water at physiological ionic strength to load the coil. The VOI size and position (in the coil and the magnet) were chosen to be similar to the in vivo studies in order to sample the B1 profile of the coil closely in (1)

$$C_{ikm} = \frac{C_i^{vitro}}{S_{iR}} \cdot \frac{\sum_j S'_{ijk} \cdot M_{jm}}{\sum_j M_{jm}} \cdot \frac{V_k^{180^\circ}}{V_R^{180^\circ}} \cdot f_i \quad \text{mM} \qquad (1);$$

$$f_i = \frac{\exp\left(-TE/T_{2i}^{vitro}\right)}{\exp\left(-TE/T_{2i}^{vivo}\right)} \cdot \frac{1-\exp\left(-TR/T_{1i}^{vitro}\right)}{1-\exp\left(-TR/T_{1i}^{vivo}\right)} \qquad (2)$$

where S_{iR} is the average signal of the *i*-th metabolite in the phantom in the same unites as S'_{ijk}, $V_k180°$ and $V_R180°$ are the RF voltage into 50 omega required for a non-selective 1 ms 180° inversion pulse on the k-th measurement and reference. The C_{imk}-*s* were corrected for *in vivo* ($T1_i^{vivo}$, $T2_i^{vivo}$) and *in vitro* ($T1_i^{vitro}$, $T2_i^{vitro}$) relaxation time differences (2). Quantification of metabolic concentrations in the ROI-s is in Table 1.

Conclusion: This study introduces an automated post-processing protocol for co-registering individual ^{1}H-MRSI data sets into the standard space and conduct data-driven voxelwise analysis with no requirement for whole-brain acquisition. It offers six main advantages: *(i)* Minimal operator intervention-with all intermediate results available for inspection; *(ii)* Minimization of repositioning errors; *(iii)* Utilization of all the voxels in the data without loss of localization resolution; (iv) Reduced "hypothesis errors" that *(v)* facilitate additional hypothesis discovery; *(vi)* Elimination of ROI position and size errors; and *(vii)* Possibility to integrate the ^{1}H-MRSI data with other imaging modalities on a voxelwise basis, e.g., PET, fMRI, taken at different times and frames of reference. Furthermore, we also provided quantification of 15 deep brain structures with this protocol, the values of which can be used to estimate effect size, power and sample size for future studies.

Reference

1. Goelman, G., Liu, S., Hess, D., Gonen, O., 2006. Optimizing the efficiency of high-field multivoxel spectroscopic imaging by multiplexing in space and time. Magn Reson Med 56, 34-40.

2. Soher, B.J., Young, K., Govindaraju, V., Maudsley, A.A., 1998. Automated spectral analysis III: application to in vivo proton MR spectroscopy and spectroscopic imaging. Magn Reson Med 40, 822-831.

3. Talairach, J., Tournoux, P., 1988. Co-planar stereotaxic atlas of the human brain: 3-dimensional proportional system: an approach to cerebral imaging. Thieme.